Heliyon 10 (2024) e32819

Contents lists available at ScienceDirect

Heliyon

journal homepage: www.cell.com/heliyon

Research article

Performance of calcium quantifications on low-dose photon-counting detector CT with high-pitch: A phantom study

Shanshui Zhou [a,b,1], Peng Liu [a,1], Haipeng Dong [a], Jiqiang Li [a], Zhihan Xu [c], Bernhard Schmidt [d], Shushen Lin [c], Wenjie Yang [a], Fuhua Yan [a,b,**], Le Qin [a,*]

[a] Department of Radiology, Ruijin Hospital, Shanghai Jiao Tong University School of Medicine, No. 197 Ruijin Er Road, Shanghai, 200025, China
[b] Faculty of Medical Imaging Technology, College of Health Science and Technology, Shanghai Jiao Tong University School of Medicine, No. 150 Ruijin Er Road, Shanghai, 200025, China
[c] Siemens Healthineers, 399 West Haiyang Road, Shanghai, 200126, China
[d] Siemens Healthineers, Siemensstrasse 3, 91301 Forchheim, Erlangen, Germany

ARTICLE INFO

Keywords:
Computed tomography
Photon-counting CT
High-pitch
Low dose
Calcium quantification

ABSTRACT

Purpose: To evaluate the performance of calcium quantification on photon-counting detector CT (PCD-CT) with high-pitch at low radiation doses compared to third-generation dual-source energy-integrating detector CT (EID-CT).

Materials and methods: The phantom with three calcium inserts (50, 100, and 300 mg of calcium per milliliter), with and without the elliptical outer layer, was evaluated using high-pitch (3.2) and standard pitch (0.8) on PCD-CT, and standard pitch on EID-CT. Scans were performed with different tube voltages (PCD-CT: 120 and 140 kilo-voltage peak [kVp]; EID-CT: 70/Sn150 and 100/Sn150 kVp) and four radiation doses (1, 3, 5, and, 10 milli-Gray [mGy]). Utilizing the true calcium concentrations (CC_{true}) of the phantom as the gold standard references, regression equations for each kVp setting were formulated to convert CT attenuations (CaCT) into measured calcium concentrations (CC_m). The correlation analysis between CaCT and CC_{true} was performed. The percentage absolute bias (PAB) was calculated from the differences between CC_m and CC_{true} and used to analyze the effects of scanning parameters on calcium quantification accuracy.

Results: A strong correlation was found between CaCT and CC_{true} on PCD-CT ($r > 0.99$) and EID-CT ($r > 0.98$). For high- and standard-pitch scans on PCD-CT, the accuracy of calcium quantification is comparable ($p = 0.615$): the median (interquartile range [IQR]) of PAB was 5.59% (2.79%–8.31%) and 4.87 % (2.62%–8.01%), respectively. The PAB median (IQR) was 7.43% (3.77%–11.75%) for EID-CT. The calcium quantification accuracy of PCD-CT is superior to EID-CT at the large phantom (5.46% [2.68%–9.55%] versus 9.01% [6.22%–12.74%]), and at the radiation dose of 1 mGy (4.43% [2.08%–8.59%] versus 13.89% [8.93%–23.09%]) and 3 mGy (4.61% [2.75%–6.51%] versus 9.97% [5.17%–14.41%]), all $p < 0.001$.

Conclusions: Calcium quantification using low-dose PCD-CT with high-pitch scanning is feasible and accurate, and superior to EID-CT.

* Corresponding author. No.197 Ruijin Er Road, Shanghai, 200025, China.
** Corresponding author. No.197 Ruijin Er Road, Shanghai 200025, China.
E-mail addresses: yfh11655@rjh.com.cn (F. Yan), ql11880@rjh.com.cn (L. Qin).
[1] Shanshui Zhou and Peng Liu made equal contributions to the work.

https://doi.org/10.1016/j.heliyon.2024.e32819
Received 5 December 2023; Received in revised form 9 June 2024; Accepted 10 June 2024
Available online 10 June 2024

1. Introduction

Dual-energy CT (DECT), allows the differentiation and quantification of various materials by comparing CT values obtained at two different energy levels [1,2]. This is valuable for quantifying iodine and calcium in clinical practice. DECT is a useful means of accurately depicting coronary artery calcium scores [3,4], determining the composition of urinary stones [5–7], and quantifying bone mineral density (BMD) [8,9].

Abbreviations

EID-CT	energy-integrating detector CT
PCD-CT	photon-counting detector CT
$CTDI_{vol}$	CT dose index volume
CaCT	calcium attenuation
CC_m	measured calcium concentration
CC_{true}	true calcium concentration
PAB	percentage absolute bias
HU	Hounsfield Units
RMSE	root-mean-squared error

As one of the latest technological advances in CT imaging, the first-generation clinically dual-source photon-counting detector CT (PCD-CT) enables energy analysis in entirely new ways. It can count X-ray photons with various energies by setting different energy thresholds. The novel construction of PCDs allows direct conversion of X-rays to electrical signals proportional to their energy levels and eliminates low-level electronic noise improving CT value stability [10,11]. Therefore, PCD-CT is able to acquire spectral information intrinsically. These features equip PCT-CT with enhanced energy separation, reduced spectral overlap, and routine output spectral information than energy-integrating detector CT (EID-CT), potentially improving the accuracy of quantifying analysis [12–14]. Another advantage of the advanced detector structure of PCD-CT is the higher geometric dose efficiency enabled by the absence of additional separation layers between individual detector cells [15]. This unique feature potentially allows the acquisition of high-quality images at lower radiation doses.

Many studies have investigated the performance of calcium measurement according to CT attenuation [16–18], but relatively few have focused on calcium quantification based on material decomposition. Some studies have illustrated that dual-energy EID-CT achieves high accuracy in calcium quantification and is even more accurate than quantitative CT (QCT) [19–21]. However, the energy spectrum images cannot be acquired using high-pitch scanning mode with pitch values higher than 1.53 on EID-CT [22]. Nevertheless, PCD-CT has the potential to apply high-pitch scanning and low doses for energy analysis due to its unique features. To the best of our knowledge, there has been no comprehensive evaluation of the calcium quantification performance of PCD-CT with high-pitch scanning at low doses before the present study.

Thus, we hypothesized that the high-pitch scanning on PCD-CT enables accurate calcium quantification at low radiation doses. Our study aimed to investigate the performance of calcium quantification using high-pitch scanning on PCD-CT at low doses. A dual-source

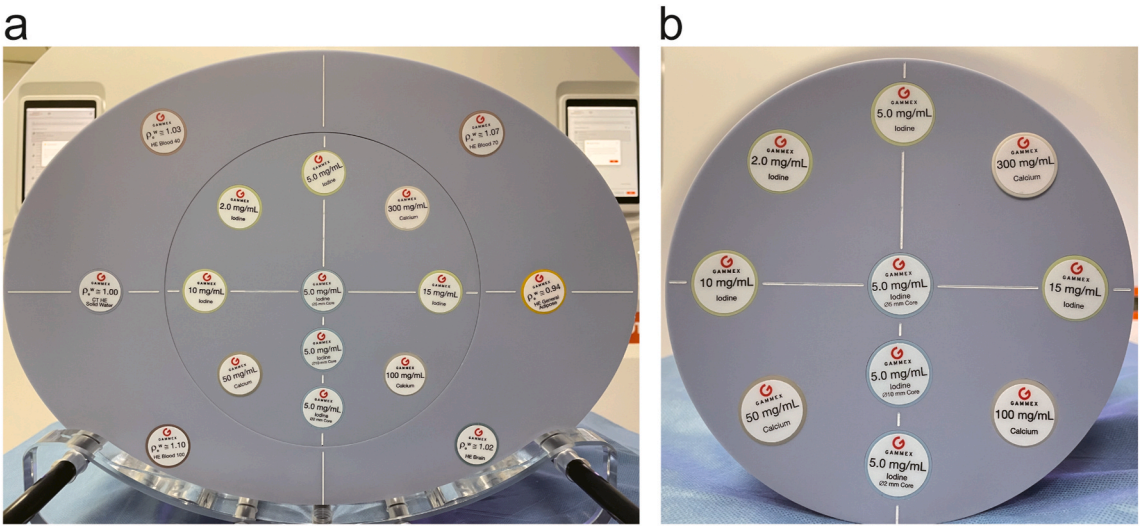

Fig. 1. The large phantom (*a*) and the small phantom (*b*) correspond to the phantom with and without the elliptical outer layer, respectively.

EID-CT was employed for the comparison analysis.

2. Materials and Methods

The institutional review board approval requirement was waived because this phantom study included no human or animal participants. The authors held full control of all the data and information submitted for publication.

2.1. Phantom

We employed a Gammex 1472 multienergy CT phantom (Sun Nuclear, Middleton, Wis, USA) comprising a 20 cm diameter cylinder for simulating smaller parts of the anatomy and a 40 × 30 cm^2 elliptical outer layer that can be placed around the cylinder to mimic larger anatomy. The phantom included 16 holes drilled to a depth of 16.5 cm, enabling the insertion of rods with simulated tissue and other biological materials, such as iodine and calcium. The primary scanning region of this phantom was 16.0 cm, with a 0.5 cm region containing the inserts and stoppers.

The phantom was used to simulate two clinical conditions, one with an elliptical outer layer of epoxy resin with a soft tissue background (large phantom, Fig. 1[a]) and one without the outer layer (small phantom, Fig. 1[b]), to represent patients of varying body sizes. The phantom contained three calcium inserts of varying concentrations (50, 100, and 300 mg/ml calcium and water mixture), all of which were of the same size and distance from the phantom center. Other inserts, such as iodine, brain, blood, adipose, and solid water, were also used to ensure that the phantom mimicked the human body as closely as possible, but these inserts were not employed for data analysis purposes.

2.2. CT examinations

Images were acquired using a first-generation clinically dual-source PCD-CT, NAEOTOM Alpha (Siemens Healthineers, Forchheim, Germany, SW version VA50, SP1) and a third-generation dual-source EID-CT, SOMATOM Force (Siemens Healthineers, Forchheim, Germany, SW version VB10).

The phantom was scanned with and without the elliptical outer layer using high-pitch (3.2) and standard-pitch (0.8) on PCD-CT. Two tube voltages of 120 and 140 kVp and four radiation doses (1, 3, 5, and 10 mGy) were employed. Each scan setting was repeated three times to ensure the precision of the obtained data. Finally, 96 comprehensive scan combinations (two phantom sizes × two scanning modes × two tube voltages × four radiation doses × three) were conducted on PCD-CT for analysis. The scan parameters on EID-CT exhibited some differences from those on PCD-CT. Specifically, only a standard pitch of 0.8 was utilized, and tube voltages were set to 70/Sn150 and 100/Sn150kVp. A total of 48 scans (two phantom sizes × two tube voltages × four radiation doses × three) were conducted on EID-CT.

For PCD-CT, the reconstructed slice thickness and increment were 0.8 and 0.6 mm, respectively, using a convolutional kernel of Qr40. The EID-CT images were reconstructed with a slice thickness of 0.75 mm, an increment of 0.6 mm, and a convolutional kernel of Qr40. Fifty to sixty percent of the maximum strength of the iterative reconstruction algorithm was utilized. Specifically, a quantum iterative reconstruction (QIR) level of two was applied on PCD-CT, while an advanced modeled iterative reconstruction (ADMIRE) level of three was employed on EID-CT.

The scanning and reconstruction parameters of the two scanners are shown in Table 1.

2.3. Image analysis

The images were transferred to the post-processing *syngo*.via, version VB70 (Siemens Healthineers, Germany) workstation for quantitative analysis of calcium concentrations. Calcium maps were generated using three-material decomposition through the Virtual Unenhanced workflow, with calcium ratios adjusted to 1.55 (for 120 kVp) and 1.67 (for 140 kVp) on PCD-CT, and 2.01 (for 70/Sn150 kVp) and 1.53 (for 100/Sn150 kVp) on EID-CT. The circular regions of interest (ROIs) with areas of 3.0 cm^2 were drawn on each calcium insert at calcium map, and the calcium attenuation (CaCT) of the respective inserts was recorded as Hounsfield Units (HU).

Table 1
Scanning and reconstruction parameters of PCD-CT and EID-CT. PCD-CT = photon-counting detector CT; EID-CT = energy-integrating detector CT; kVp = kilo-voltage peak; IR = iterative reconstruction; QIR = Quantum iterative reconstruction; ADMIRE = advanced modeled iterative reconstruction.

	PCD-CT	EID-CT
Tube voltage (kVp)	120	70/Sn150
	140	100/Sn150
Scanning pitch	3.2 and 0.8	0.8
Collimation (mm)	144 × 0.4	128 × 0.6
Rotation time (s)	0.25	0.28
Slice thickness/increment (mm)	0.8/0.6	0.75/0.6
Kernel	Qr40	Qr40
IR algorithms and strength	QIR: 2	ADMIRE: 3

One radiologist with >10 years of experience performed all measurements, carefully avoiding the effects of beam hardening artifacts. To avoid errors caused by ROI inconsistencies, we applied the copy-and-paste function on the workstation to maintain constant ROI sizes, shapes, and positions across all images for each scan setting. The results of the measurements, taken across three consecutive

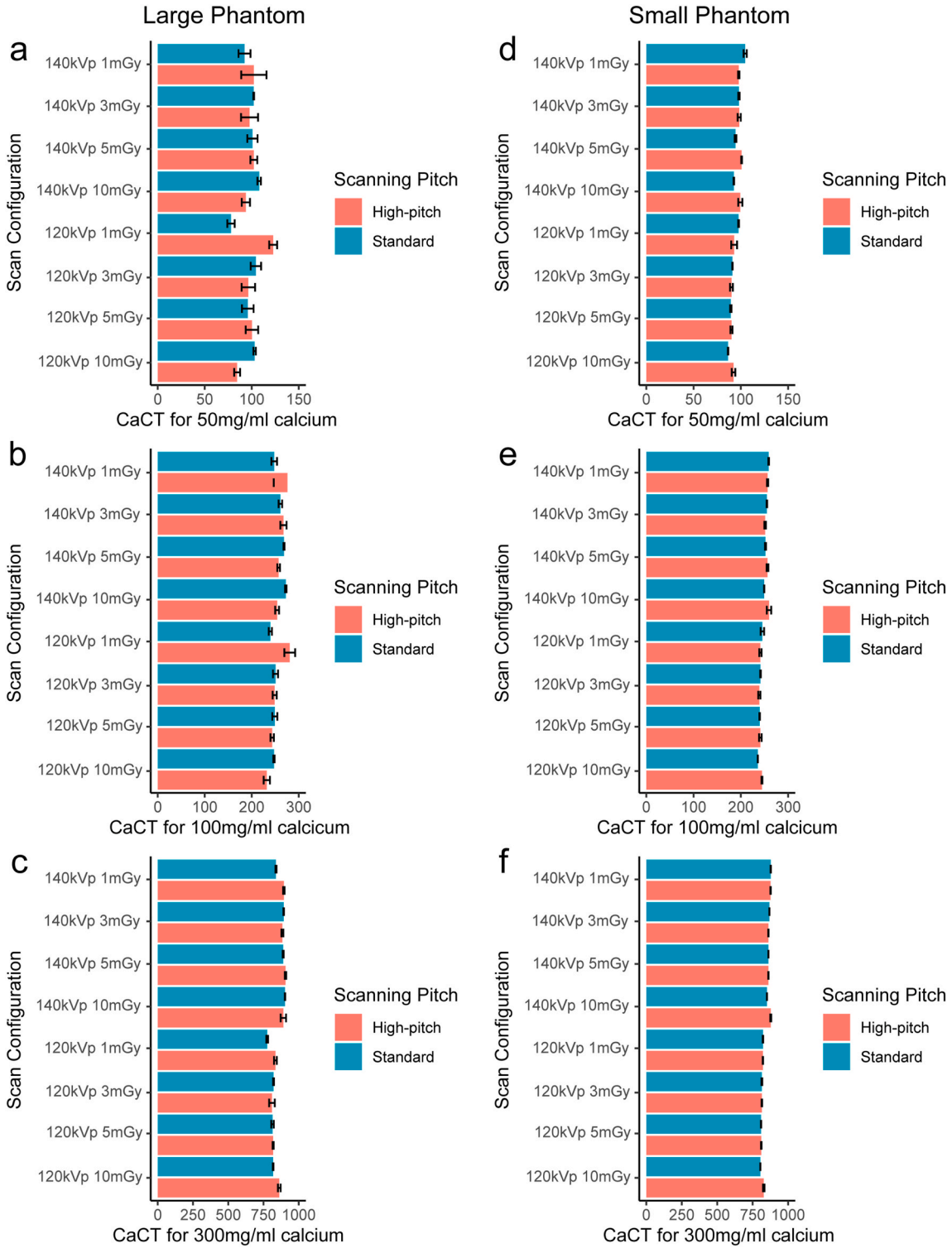

Fig. 2. Calcium attenuation measurement for all scan settings. *a–c*: 50, 100, and 300 mg/ml calcium placed into the large phantom; *d–f*: 50, 100, and 300 mg/ml calcium placed into the large phantom. *CaCT = calcium attenuation measured on Calcium maps.*

slices, were averaged for error analysis ensuring the highest standards of precision and reliability. We reference the methodology proposed by Symons et al. [23], defining the stability of HU values on PCD-CT and EID-CT as the difference in HU measured at 10-mGy and 1-mGy for each tube voltage.

2.4. Calcium concentration

Since currently there is no reference equation for converting CaCT to calcium concentration, the equations between CaCT and true calcium concentration (CC_{true}) were derived by the linear regression analysis [24–26]. Some studies utilized a similar method to evaluate the calcium quantification accuracy of EID-CT [9,20]. The reference CaCT is measured on images of the small phantom scanned at the pitch of 0.8 with 10 mGy while CC_{true} is the gold standard reference provided by the phantom manufacturer. As the flux of X-rays exhibits variation in response to alterations in tube voltage settings, we performed this step separately for each kVp setting. Then, the CaCT was converted to measured calcium concentrations (CC_m) based on regression equations.

Bias was defined as the result of CC_m minus CC_{true}. Using CC_{true} as the gold standard reference, the percentage absolute bias (PAB) was determined for each insert and acquisition, simulating the methodology of relative measurement error described in Ref. [27], through the following calculation:

$$PAB = \frac{|CC_m - CC_{true}|}{CC_{true}} \times 100\%$$

2.5. Statistical analysis

Kolmogorov–Smirnov tests were performed to evaluate data normality. Normally distributed continuous variables are presented as mean ± standard deviation (SD), whereas variables with skewed distributions are presented as median (interquartile range [IQR]). Linear regression and Pearson's correlation coefficients were employed to investigate the correlations between CaCT and CC_{true} for all scan settings. To evaluate the overall accuracy of PCD-CT, the total error of the CC_m was defined as the root-mean-squared error (RMSE) across the inserts. This was calculated based on each equation of CaCT converted into CC_m. The Friedman test was used to

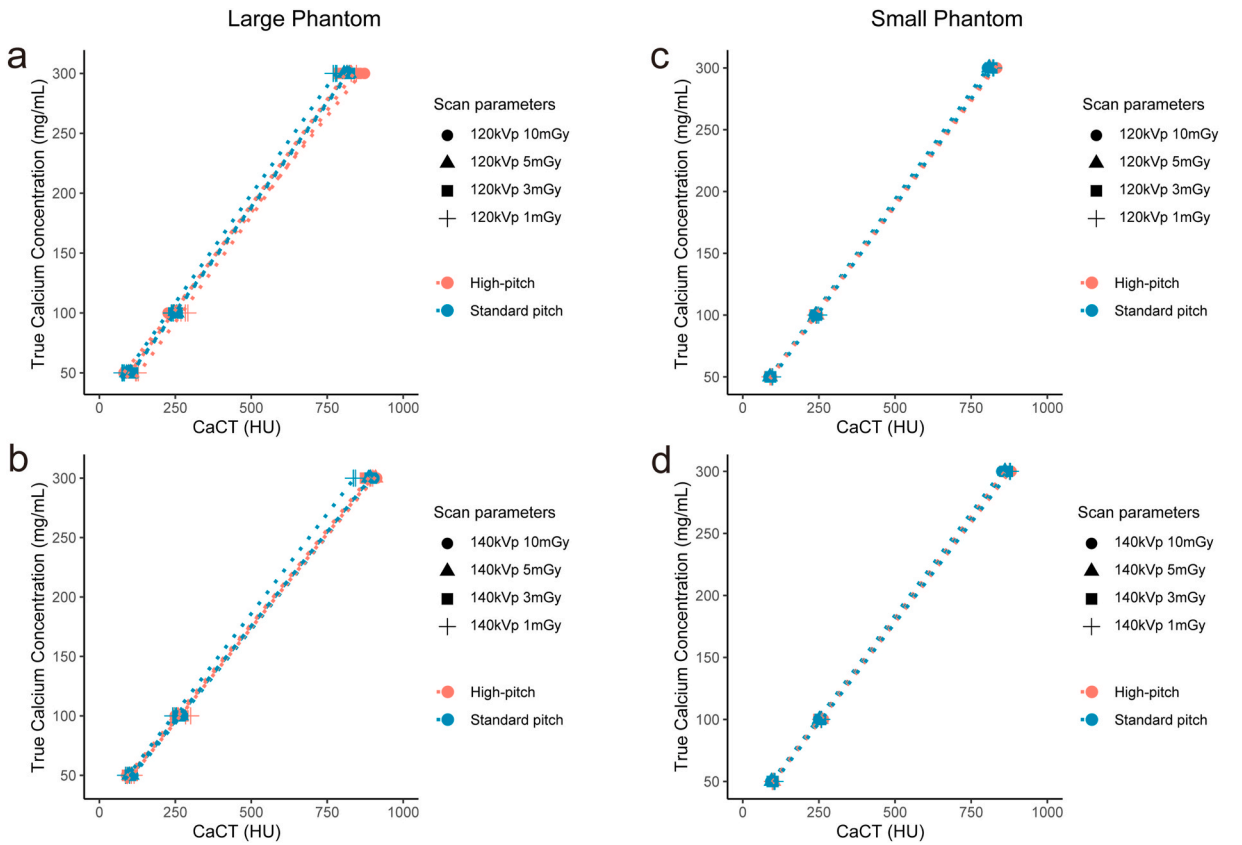

Fig. 3. Linear regression showed strong correlation between calcium attenuation and true calcium concentrations for all scan settings on PCD-CT. *a and b*: the large phantom scanned at 120 kVp (*a*) and 140 kVp (*b*); *c and d*: the small phantom scanned at 120 kVp (*c*) and 140 kVp (*d*). *CaCT = calcium attenuation measured on Calcium maps.*

compare the differences in bias and PAB between the four radiation dose groups. The Wilcoxon signed-rank test was used to compare the differences between the scanning mode and phantom size groups. A mixed-effect linear regression analysis was performed for PAB to further explore the effects of scanning modes, phantom sizes, tube voltages, and the interactions between scanning modes and radiation doses on quantitative accuracy. R software (version 4.3.0) was used for all statistical analyses. A p-value <0.05 was considered statistically significant.

3. Results

3.1. Calcium attenuation

For PCD-CT, the measured CT values of inserts with 50, 100, and 300 mg of calcium per milliliter at the Calcium maps are presented as mean (range) values. For the large phantom (Fig. 2[a–c]), these values were 98.99 (74.27–127.50), 255.99 (226.20–300.67), and 853.33 (769.4–912.67) HU, respectively. In contrast, the small phantom (Fig. 2[d–f]) yielded CT values of 94.72 (86.23–105.83) HU, 248.01 (235.70–264.90) HU, and 841.18 (803.70–880.90) HU, respectively. The measured CT values of calcium inserts with concentrations of 50, 100, and 300 mg/ml were 113.49 (94.80–139.30), 315.10 (248.40–459.50), and 1055.90 (912.40–1294.60) HU for large phantom and 97.05 (86.40–105.70), 279.82 (250.40–313.20), and 1047.61 (940.10–1165.70) HU for small phantom on EID-CT.

For HU stability, PCD-CT is superior to EID-CT in certain scenarios. The means ± SD of the differences between CT values at 10-mGy and 1-mGy of 50, 100, and 300 mg/ml calcium inserts at 120 kVp on PCD-CT and 70/150Sn kVp on EID-CT were -6.24 ± 23.85 HU versus (vs.) 3.18 ± 14.91 HU ($p = 0.258$), -11.82 ± 23.90 HU vs. -42.40 ± 72.44 HU ($p = 0.188$), 14.22 ± 24.18 HU vs. 74.66 ± 45.27 HU ($p < 0.001$). At 140 kVp of PCD-CT and 100/Sn150 kVp of EID-CT, these values were -0.83 ± 12.83 HU vs. -18.19 ± 7.26 HU ($p < 0.001$), -0.98 ± 21.27 HU vs. -11.53 ± 8.32 HU ($p = 0.131$), 8.59 ± 36.33 HU vs. -51.52 ± 40.42 HU ($p = 0.001$). The percentages of mean HU differences relative to the measured mean HU values for 50, 100, and 300 mg/ml calcium on PCD-CT were −6.60%, −4.83%, and 1.73% under 120 kVp and −0.83%, −0.38%, and 0.98% under 140 kVp, respectively. In contrast, these percentages on EID-CT were 3.04%, −12.61%, and 6.70% under 70/Sn150 kVp and −17.52%, −4.31%, and −5.34% under 100/Sn150 kVp, respectively.

Linear regression analysis results of PCD-CT and EID-CT are shown in Fig. 3[a–d] and Fig. 4[a–d], respectively. There are extremely strong correlations between CaCT and CC_{true} for all scan settings on PCD-CT (all $r > 0.99$). The comparable strong correlations between

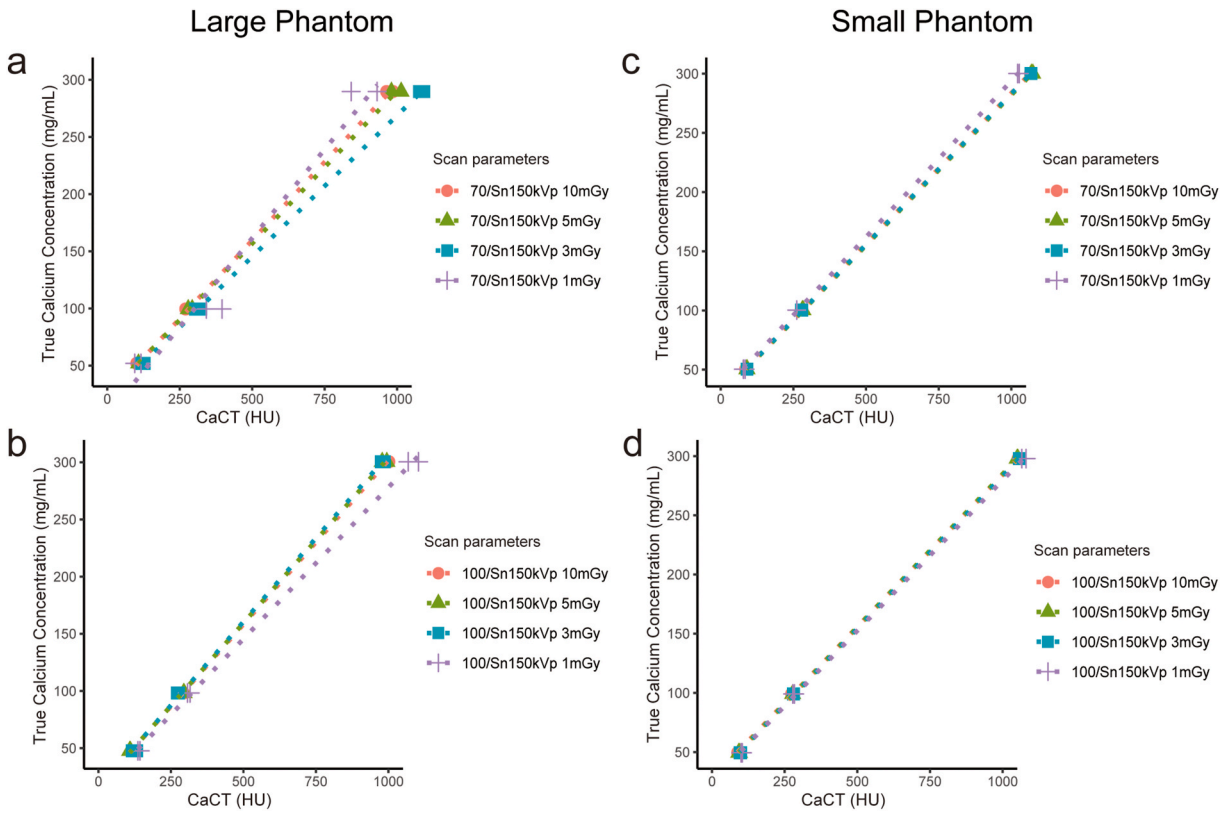

Fig. 4. Linear regression showed strong correlation between calcium attenuation and true calcium concentrations for all scan settings on EID-CT. *a and b*: the large phantom scanned at 70/Sn150 kVp (*a*) and 100/Sn150 kVp (*b*); *c and d*: the small phantom scanned at 70/Sn150 kVp (*c*) and 100/Sn150 kVp (*d*). *CaCT = calcium attenuation measured on Calcium maps.*

CaCT and CC_{true} on EID-CT were observed (all $r > 0.98$). On PCD-CT and EID-CT, the median (IQR) of the conversion slope of the linear regression lines was 0.328 (0.316–0.350) and 0.276 (0.237–0.303) mg/ml/HU for the large phantom and 0.326 (0.336–0.346) and 0.267 (0.237–0.292) mg/ml/HU for the small phantom, respectively. The standard deviations for the slopes of the large and small phantoms were 0.182 and 0.108 on PCD-CT and 0.344 and 0.282 on EID-CT, respectively. The regression lines for each scan setting in the large phantom (Fig. 3[a, b] and Fig. 4[a, b]) were noticeably more discrete than those in the small phantom (Fig. 3[c, d] and Fig. 4 [c, d]).

3.2. Calcium concentration

For PCD-CT, the reference equations for the conversion of CaCT into CC_m were $y = 18.82 + 0.35x$ and $y = 18.61 + 0.33x$ for all scans at tube voltages of 120 and 140 kVp, respectively. For the inserts of 50, 100, and 300 mg/ml calcium, the median (IQR) of CC_m was 52.25 (48.86–54.14), 105.91 (99.27–108.32), and 310.12 (291.14–322.09) mg/ml, respectively. Bias between CC_m and CC_{true} was 2.25 (−1.14–4.14), 5.91 (−0.73–8.32), and 10.12 (−8.86–22.09) mg/ml, and PAB was 5.51% (2.75%–8.45%), 5.91% (2.36%–8.32%), and 4.66% (2.94%–7.36%), respectively. Scans with PABs larger than 10% and 20% accounted for 16.67% and 1.74% of all scans in this study, respectively. The box plot of PAB values corresponding to 120 and 140 kVp on PCD-CT is shown in Fig. 5[a, b].

The reference equations for converting CaCT into CC_m were $y = 26.76 + 0.24x$ and $y = 25.32 + 0.29x$ for scans with tube voltage of 70/Sn150 and 100/Sn150 kVp on EID-CT. For the inserts of 50, 100, and 300 mg/ml calcium, the bias was 4.95 (1.59–10.03), 6.14 (−3.71–9.31), and 0.21 (−14.09–20.61) mg/ml and PAB was 8.24% (6.22%–9.82%), 6.14% (3.33%–14.41%), and 6.76% (3.14%–12.74%), respectively. Scans with PABs larger than 10% and 20% accounted for 30.21% and 13.54%, respectively. The box plot of PAB values of all scans on EID-CT is shown in Fig. 6.

3.3. Root-mean-squared error

The median (IQR) RMSEs were 1.25 (0.81–2.75) and 0.90 (0.68–1.50) for high- and standard-pitch scanning, respectively. The largest RMSE of 5.35 was obtained with the large phantom scanned with high pitch at 140 kVp and 1 mGy, whereas the smallest of 0.34 was the small phantom scanned obtained with standard pitch at 140 kVp and 1 mGy. Fig. 7 illustrates that the RMSEs of the small phantom were more accurate than those of the large one, and the differences between high- and standard-pitch scanning were lower in the small than the large phantom.

3.4. Errors analysis

For scans at radiation doses of 1, 3, 5, and 10 mGy, the median (IQR) of PABs on PCD-CT were 4.43% (2.08%–8.59%), 4.61% (2.75%–6.51%), 5.88% (3.35%–8.33%), and 5.59% (2.62%–8.65%). The statistical difference is not observed ($p = 0.321$) (Table 2). For EID-CT, the PAB values of scans at 1, 3, 5, and 10 mGy were 13.89% (8.93%–23.09%), 9.97% (5.17%–14.41%), 4.48% (3.50%–6.68%), and 2.73% (0.65%–9.13%). The statistical difference in PAB was observed between radiation doses ($p < 0.001$) (Table 3). Table 4 shows that PCD-CT is superior to EID-CT at 1 and 3 mGy (all $p < 0.001$) while similar at 5-mGy ($p = 0.246$) and 10-mGy ($p = 0.059$).

The obvious diversities were observed between the large and small phantom groups in PAB on PCD-CT (5.46% [2.68%–9.55%] vs. 4.98% [2.75%–7.34%]; $p = 0.034$) (Table 5). There also is statistical difference in PAB between the large and small phantom on EID-CT (9.01% [6.22%–12.74%] vs. 4.48% [1.88%–10.64%]; $p < 0.001$) (Table 6). PCD-CT is superior in large phantom ($p < 0.001$) while similar in the small phantom ($p = 0.537$) compared with EID-CT (Table 7).

For the comparison of high-pitch and standard pitch on PCD-CT, Table 8 illustrates that PAB values had no statistical differences between high- and standard-pitch scans on PCD-CT (5.59% [2.79%–8.31%] vs. 4.87% [2.62%–8.01%]; $p = 0.615$).

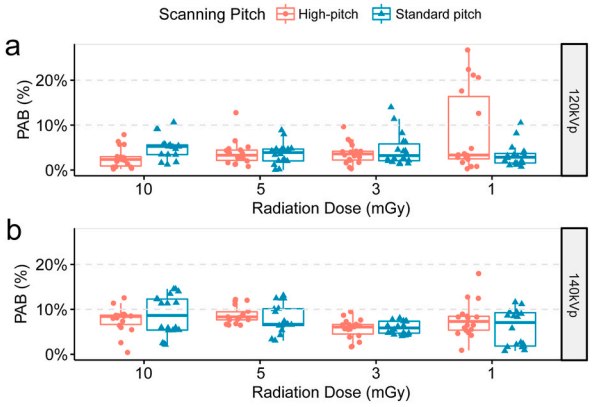

Fig. 5. The box plot of PAB for all scans on PCD-CT at 120 kVp (*a*) and 140 kVp (*b*). *PAB = percentage absolute bias.*

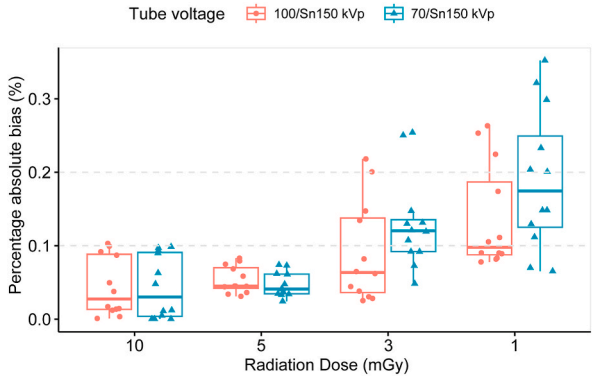

Fig. 6. The box plot of PAB for all scans on EID-CT. The scans conducted at 1- and 3-mGy regardless of the tube voltage exhibited higher PAB than other scans. *PAB = percentage absolute bias.*

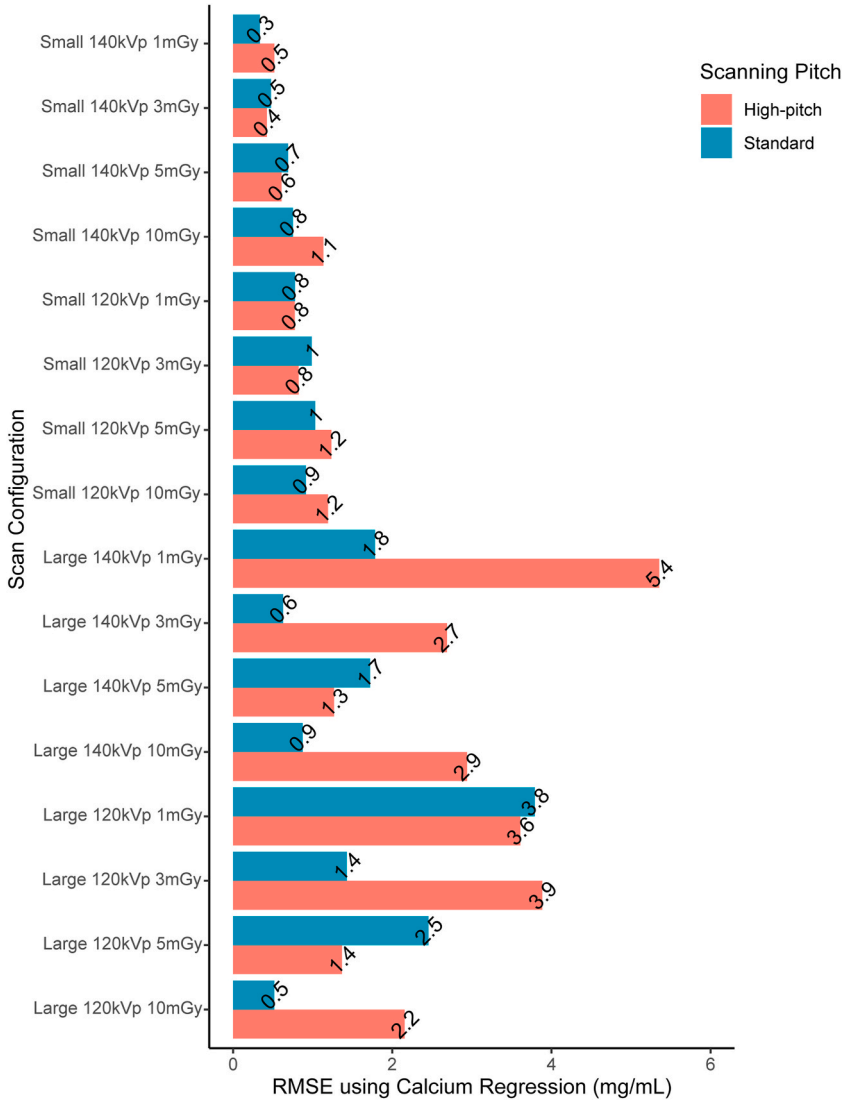

Fig. 7. RMSEs based on the equation of converting calcium attenuation into measured calcium concentration. *RMSE = root-mean-square error; Small = small phantom; Large = large phantom.*

Table 2
Comparison of bias and PAB of measured calcium concentrations using PCD-CT to the true calcium concentrations among different radiation doses. PAB = percentage absolute bias; PCD-CT = photon-counting detector CT; mGy = milli-Gray.

	10 mGy	5 mGy	3 mGy	1 mGy	p value
	N = 72	N = 72	N = 72	N = 72	
Bias	4.60 [-0.71 to 11.90]	4.12 [-0.14 to 8.45]	4.13 [-1.12 to 7.40]	2.21 [-1.97 to 9.69]	0.690
PAB (%)	5.59 [2.62 to 8.65]	5.88 [3.35 to 8.33]	4.61 [2.75 to 6.51]	4.43 [2.08 to 8.59]	0.321

Table 3
Comparison of bias and PAB of measured calcium concentrations using EID-CT to the true calcium concentrations among different radiation doses. PAB = percentage absolute bias; EID-CT = energy-integrating detector CT; mGy = milli-Gray.

	10 mGy	5 mGy	3 mGy	1 mGy	p value
	N = 36	N = 36	N = 36	N = 36	
Bias	0.45 [-1.30 to 4.96]	3.67 [-3.04 to 7.15]	8.66 [-2.52 to 12.66]	10.28 [-14.04 to 21.54]	0.010
PAB (%)	2.73 [0.65 to 9.13]	4.48 [3.50 to 6.68]	9.97 [5.17 to 14.41]	13.89 [8.93 to 23.09]	<0.001 [a]

[a] with statistical significance.

Table 4
Comparison of PAB (%) acquired at different radiation doses between PCD-CT and EID-CT. PAB = percentage absolute bias; PCD-CT = photon-counting detector CT; EID-CT = energy-integrating detector CT; mGy = milli-Gray.

	PCD-CT	EID-CT	p value
	N = 288	N = 144	
1 mGy	4.43 [2.08 to 8.59]	13.89 [8.93 to 23.09]	<0.001 [a]
3 mGy	4.61 [2.75 to 6.51]	9.97 [5.17 to 14.41]	<0.001 [a]
5 mGy	5.88 [3.35 to 8.33]	4.48 [3.50 to 6.68]	0.246
10 mGy	5.59 [2.62 to 8.65]	2.73 [0.65 to 9.13]	0.059

[a] with statistical significance.

Table 5
Comparison of bias and PAB between large and small phantoms on PCD-CT. PAB = percentage absolute bias; PCD-CT = photon-counting detector CT.

	Large	Small	p value
	N = 144	N = 144	
Bias	5.36 [2.38 to 11.30]	1.07 [-2.10 to 8.02]	<0.001 [a]
PAB (%)	5.46 [2.68 to 9.55]	4.98 [2.75 to 7.34]	0.034 [a]

[a] with statistical significance.

Table 6
Comparison of bias and PAB between large and small phantoms on EID-CT. PAB = percentage absolute bias; EID-CT = energy-integrating detector CT.

	Large	Small	p value
	N = 72	N = 72	
Bias	8.05 [-3.80 to 11.88]	1.13 [-3.71 to 8.29]	0.045 [a]
PAB (%)	9.01 [6.22 to 12.74]	4.48 [1.88 to 10.64]	0.001 [a]

[a] with statistical significance.

Results of mixed-effective linear regressions of PCD-CT showed that neither scanning modes ($p = 0.055$) nor tube voltages ($p = 0.215$) significantly affected PAB values (Table 9). However, the PAB values of the small phantom scans were 3.70% smaller than those for the large phantom with the same scan settings ($p = 0.023$). In addition, compared to 10 mGy scans, 1 mGy scans obviously affected PAB ($p = 0.010$). The interaction analysis revealed that, in the high-pitch scanning conditions, the 1 mGy scan led to a noteworthy 2.20% ($p = 0.010$) increase in the PAB obtained for the 10 mGy scan. Nevertheless, in standard-pitch scanning, this variance was mitigated, with a correction of 4.10% ($p < 0.001$). For EID-CT, results of mixed-effective linear regressions showed that PAB was significantly affected by the phantom size ($p < 0.001$) and low radiation doses of 1 and 3-mGy (all $p < 0.001$) (Table 10).

Table 7
Comparison of PAB (%) acquired at different phantom sizes between PCD-CT and EID-CT. PAB = percentage absolute bias; PCD-CT = photon-counting detector CT; EID-CT = energy-integrating detector CT.

	PCD-CT	EID-CT	p value
	N = 288	N = 144	
Large	5.46 [2.68 to 9.55]	9.01 [6.22 to 12.74]	<0.001 [a]
Small	4.98 [2.75 to 7.34]	4.48 [1.88 to 10.64]	0.537

[a] with statistical significance.

Table 8
Comparison of bias and PAB between standard- and high-pitch on PCD-CT. PAB = percentage absolute bias; PCD-CT = photon-counting detector CT.

	High-pitch	Standard pitch	p value
	N = 144	N = 144	
Bias	4.12 [-0.82 to 9.82]	3.60 [-1.54 to 7.29]	0.121
PAB (%)	5.59 [2.79 to 8.31]	4.87 [2.62 to 8.01]	0.615

Table 9
Mixed-effect linear regression analysis for PAB across different scanning parameters on PCD-CT. PAB = percentage absolute bias; PCD-CT = photon-counting detector CT; kVp = kilo-voltage peak; mGy = milli-Gray.

		Estimate	Standard error	p value
	(Intercept)	0.057	0.007	<0.001 [a]
Scanning Mode	**High-pitch**	–	–	–
	Standard pitch	0.017	0.009	0.055
Tube voltage	**120 kVp**	–	–	–
	140 kVp	0.005	0.004	0.215
Radiation dose	**10 mGy**	–	–	–
	5 mGy	0.010	0.009	0.229
	3 mGy	−0.009	0.009	0.282
	1 mGy	0.022	0.009	0.010 [a]
Phantom Size	**Large**	–	–	–
	Small	−0.037	0.004	0.023 [a]
Interaction	**Standard: 10 mGy**	–	–	–
	Standard: 5 mGy	−0.021	0.012	0.084
	Standard: 3 mGy	−0.016	0.012	0.196
	Standard: 1 mGy	−0.041	0.012	<0.001 [a]

[a] with statistical significance.

4. Discussion

In this study, we used a multienergy phantom to evaluate the performance of calcium quantification using high-pitch scanning on PCD-CT at low radiation doses, and dual-source EID-CT was employed for comparison analysis. The phantom size, tube voltage, and radiation dose were assessed as measures of the effects of body shape, X-ray energy, and radiation quantity on the calcium analysis outcomes. The results of our study suggest the following: (1) Calcium concentrations can be accurately quantified using PCD-CT at low radiation doses; (2) High-pitch scanning produces equivalent calcium quantification accuracy to standard-pitch scanning on PCD-CT; (3) The quantification accuracy of PCD-CT is superior to EID-CT at large phantom and radiation doses of 1- and 3-mGy.

The HU stability of PCD-CT and EID-CT was assessed before evaluating the accuracy of calcium quantification. The differences between HU values measured at 10-mGy and 1-mGy are always below 15 HU on PCD-CT. Moreover, the percentage of this HU deviation relative to the measured mean HU value consistently remained under 10% (range: 0.38%–6.60%). In contrast, EID-CT exhibited HU differences ranging from 3.18 to 74.66 HU, with corresponding percentage deviations relative to mean HU values ranging from 3.04% to 17.52%. The stability of HU values is superior in PCD-CT compared to EID-CT in certain scans, which is consistent with the finding of [23]. The stability of HU values on PCD-CT under varying scanning parameters lays the foundation for the evaluation of calcium quantification.

Several studies have examined the calcium quantification accuracy of EID-CT. Mei et al. examined the accuracy of quantifying calcium hydroxyapatite (HA) concentrations of 100, 200, 400, and 800 mg/cm^3 using a dual-layer spectral CT. They conducted their study at a radiation dose range of 1.2–63.1 mGy with a scanning pitch of 1.058, and the measurement error ranged from −1.26% to 14.84% [28]. Van Hamersvelt et al. obtained mean relative measurement errors of -1.8 ± 4.0 %, -2.9 ± 2.6 %, and -5.3 ± 2.7 % for 120 kVp and 3.1 ± 2.1 %, -0.7 ± 1.7 %, and -2.9 ± 1.3 % for 140 kVp with HA quantifications of 50, 100, and 200 mg/cm^3, respectively. The scanning pitch was 0.925 and radiation doses were 4.5–18.1 mGy for 120 kVp and 6.5–26.0 mGy for 140 kVp. They

Table 10
Mixed-effect linear regression analysis for PAB across different scanning parameters on EID-CT. PAB = percentage absolute bias; EID-CT = integrating detector CT; kVp = kilo-voltage peak; mGy = milli-Gray.

		Estimate	Standard error	p value
	(Intercept)	0.056	0.013	<0.001 [a]
Tube voltage	**100/Sn150kVp**	–	–	–
	70/Sn150kVp	0.022	0.011	0.052
Radiation dose	**10 mGy**	–	–	–
	5 mGy	0.007	0.016	0.676
	3 mGy	0.066	0.016	<0.001 [a]
	1 mGy	0.120	0.016	<0.001 [a]
Phantom Size	**Large**	–	–	–
	Small	−0.047	0.011	<0.001 [a]

[a] with statistical significance.

found that the errors increased at the lowest radiation dose, and statistically significant differences were observed between the protocols utilizing higher doses and those using the lowest dose [27]. Compared with the aforementioned studies, the present study employed PCD-CT at lower radiation doses of 1–10 mGy but achieved comparable calcium quantification accuracy. The median (IQR) of PAB values were 5.51% (2.75%–8.45%), 5.91% (2.36%–8.32%), and 4.66% (2.94%–7.36%) for 50, 100, and 300 mg/ml calcium, respectively. In contrast, EID-CT at the same radiation doses exhibited higher PAB of 8.24% (6.22%–9.82%), 6.14% (3.33%–14.41%), and 6.76% (3.14%–12.74%) for the three calcium inserts. This may be attributed to the excellent geometric dose efficiency and the availability of more abundant energy spectrum information with PCD-CT [29,30]. Because calcium has a large atomic number and bones have high calcium content, the photoelectric effect increased when the X-rays passed. Typically, the radiation dose of skeletal CT imaging was likely to be significantly higher than that for the soft tissue [31]. Nevertheless, Grunz et al. have suggested that PCD-CT enables high-resolution bone imaging at lower radiation doses. Our study confirmed that, beyond structural imaging, accurate calcium quantification using PCD-CT can be conducted with lower radiation doses [32].

In this study, bias and PAB were significantly different between the two phantom sizes. Scans performed with the large phantom exhibited greater bias and PAB values than those that used the small phantom. We also found significant disparities between the PAB values of 10 mGy and 1 mGy radiation doses but not between those of the 10 mGy and 3 mGy or the 10 mGy and 5 mGy scans on PCD-CT. This difference is likely due to the low radiation dose employed and the absorption of some of the X-ray energy by the outer phantom. Ohira et al. [33] have pointed out that deficient levels of radiation output will produce less accurate quantifications when scanning a large phantom. Therefore, we believe that a higher radiation dose (>3 mGy in this study) is needed for calcium quantification of extensive scanning areas, such as the abdomen, to ensure sufficient accuracy. Although scanning pitch does not affect the accuracy of calcium quantification, interaction analysis has revealed that high-pitch scanning leads to a higher PAB than standard-pitch scanning at 1 mGy. It may be due to ultra-low radiation doses inevitably leading to reductions in both the energy and quantity of X-ray photons [34].

Scanning at a high pitch may facilitate lower radiation doses and faster scanning speeds than those at a standard pitch [35–37]. Although previous work has assessed coronary artery calcium scoring using high-pitch scanning of PCD-CT [38–40], there have been no studies of calcium quantification based on material decomposition. Our study employed lower radiation doses than previous research and there are gold standards of calcium concentration for comparison. Moreover, we demonstrated that high- and standard-pitch scanning produce comparable performance. In addition, the PAB values of both high-pitch (5.59% [2.79%–8.31%]) and standard-pitch (4.87% [2.62%–8.01%]) of PCD-CT are superior to EID-CT with standard-pitch (7.43% [3.77%–11.75%], all p = 0.001). This means that the advantages of high-pitch scans can be applied not only to regular anatomical imaging but also to quantify calcium on PCD-CT.

Our results have important clinical implications. Quantifying BMD is equivalent to quantifying HA, and calcium constitutes approximately 39.9% of the composition of HA, thus we can effectively measure BMD by quantifying calcium based on material decomposition using spectral CT [41]. Calcium quantification is important for measuring BMD in the thoracic and lumbar vertebrae with routine thoracic or abdominal CT for noninvasive and convenient osteoporosis screening [42–44]. In addition, it can be used to monitor medullary bone loss in hemodialysis patients with secondary hyperparathyroidism, as well as long-term cortical bone loss after parathyroidectomy, thus guiding further therapies [45]. Calcium quantification also enables discernment and quantification of the diverse constituents of urinary stones during extensive field-of-view CT urography [46]. This study demonstrated that PCD-CT with high-pitch scanning at low radiation doses achieved high accuracy in calcium quantification, which suggests that the above applications can be performed with faster acquisition speeds and lower radiation exposure using PCD-CT.

However, this study had several limitations. First, this was a phantom study requiring further validation with human participants. While inserts, such as calcium and iodine, can simulate skeletal and soft tissue environments, a phantom does not replicate the complexity of the human body. Second, the standard formula for converting attenuation measured on calcium maps to the true concentration remains unknown because there are no gold standard references of HU values of the phantom under varying scanning settings. Finally, we did not investigate its application in clinical practice. Further research is imperative to fully comprehend the capabilities and limitations of PCD-CT for accurate absolute calcium quantification in clinical practice.

In conclusion, high-pitch scanning on PCD-CT is a feasible approach for assessing the accuracy of calcium quantification and demonstrates superior accuracy compared to EID-CT. Nonetheless, the phantom size and extremely low doses of 1 mGy could affect

this accuracy on both PCD-CT and EID-CT. Our results may expand the clinical applications of calcium quantification on PCD-CT. However, the performance should be validated in human studies in the future.

Data availability statement

Data will be made available on request.

CRediT authorship contribution statement

Shanshui Zhou: Writing – original draft, Visualization, Validation, Methodology, Investigation, Data curation. **Peng Liu:** Writing – original draft, Visualization, Validation, Methodology, Investigation, Data curation. **Haipeng Dong:** Methodology, Investigation, Data curation. **Jiqiang Li:** Methodology, Investigation, Data curation. **Zhihan Xu:** Writing – review & editing, Visualization, Formal analysis. **Bernhard Schmidt:** Writing – review & editing, Visualization. **Shushen Lin:** Visualization, Formal analysis. **Wenjie Yang:** Writing – review & editing. **Fuhua Yan:** Writing – review & editing, Software, Resources, Methodology, Conceptualization. **Le Qin:** Writing – review & editing, Validation, Supervision, Project administration, Methodology, Investigation, Funding acquisition, Conceptualization.

Declaration of competing interest

The authors declare the following financial interests/personal relationships which may be considered as potential competing interests:

Zhihan Xu reports a relationship with Siemens Healthineers that includes: employment. Bernhard Schmidt reports a relationship with Siemens Healthineers that includes: employment. Shushen Lin reports a relationship with Siemens Healthineers that includes: employment. If there are other authors, they declare that they have no known competing financial interests or personal relationships that could have appeared to influence the work reported in this paper.

Acknowledgment

The study has received funding from 1) Natural Science Foundation of China under Grant: 82101988; 2) 2021 Shanghai Sailing Program: 21YF1426200.

References

[1] T.R.C. Johnson, Dual-energy CT: general principles, AJR Am. J. Roentgenol. 199 (5 Suppl) (2012) S3–S8, https://doi.org/10.2214/AJR.12.9116.
[2] C.H. McCollough, S. Leng, L. Yu, J.G. Fletcher, Dual- and multi-energy CT: principles, technical Approaches, and clinical applications, Radiology 276 (3) (2015) 637–653, https://doi.org/10.1148/radiol.2015142631.
[3] F. Schwarz, J.W. Nance, B. Ruzsics, G. Bastarrika, A. Sterzik, U.J. Schoepf, Quantification of coronary artery calcium on the basis of dual-energy coronary CT angiography, Radiology 264 (3) (2012) 700–707, https://doi.org/10.1148/radiol.12112455.
[4] R. Wang, W. Yu, Y. Wang, et al., Incremental value of dual-energy CT to coronary CT angiography for the detection of significant coronary stenosis: comparison with quantitative coronary angiography and single photon emission computed tomography, Int. J. Cardiovasc. Imag. 27 (5) (2011) 647–656, https://doi.org/10.1007/s10554-011-9881-7.
[5] G. Hidas, R. Eliahou, M. Duvdevani, et al., Determination of renal stone composition with dual-energy CT: in vivo analysis and comparison with x-ray diffraction, Radiology 257 (2) (2010) 394–401, https://doi.org/10.1148/radiol.10100249.
[6] A.N. Primak, J.G. Fletcher, T.J. Vrtiska, et al., Noninvasive differentiation of uric acid versus non-uric acid kidney stones using dual-energy CT, Acad. Radiol. 14 (12) (2007) 1441–1447.
[7] E.S. Wisenbaugh, R.G. Paden, A.C. Silva, M.R. Humphreys, Dual-energy vs conventional computed tomography in determining stone composition, Urology 83 (6) (2014) 1243–1247, https://doi.org/10.1016/j.urology.2013.12.023.
[8] C. Booz, J. Noeske, M.H. Albrecht, et al., Diagnostic accuracy of quantitative dual-energy CT-based bone mineral density assessment in comparison to Hounsfield unit measurements using dual x-ray absorptiometry as standard of reference, Eur. J. Radiol. 132 (2020) 109321, https://doi.org/10.1016/j.ejrad.2020.109321.
[9] S. Zhou, L. Zhu, T. You, et al., In vivo quantification of bone mineral density of lumbar vertebrae using fast kVp switching dual-energy CT: correlation with quantitative computed tomography, Quant. Imag. Med. Surg. 11 (1) (2021) 341–350, https://doi.org/10.21037/qims-20-367.
[10] T. Flohr, M. Petersilka, A. Henning, S. Ulzheimer, J. Ferda, B. Schmidt, Photon-counting CT review. Physica medica : PM : an International Journal Devoted to the applications of physics to medicine and biology, Official Journal of the Italian Association of Biomedical Physics (AIFB) 79 (2020) 126–136, https://doi.org/10.1016/j.ejmp.2020.10.030.
[11] A. Esquivel, A. Ferrero, A. Mileto, et al., Photon-counting detector CT: key points radiologists should know, Korean J. Radiol. 23 (9) (2022) 854–865, https://doi.org/10.3348/kjr.2022.0377.
[12] R. Symons, B. Krauss, P. Sahbaee, et al., Photon-counting CT for simultaneous imaging of multiple contrast agents in the abdomen: an in vivo study, Med. Phys. 44 (10) (2017) 5120–5127, https://doi.org/10.1002/mp.12301.
[13] M.J. Willemink, M. Persson, A. Pourmorteza, N.J. Pelc, D. Fleischmann, Photon-counting CT: technical principles and clinical prospects, Radiology 289 (2) (2018) 293–312, https://doi.org/10.1148/radiol.2018172656.
[14] M. Danielsson, M. Persson, M. Sjölin, Photon-counting x-ray detectors for CT, Phys. Med. Biol. 66 (3) (2021) 03TR1, https://doi.org/10.1088/1361-6560/abc5a5.
[15] S. Leng, M. Bruesewitz, S. Tao, et al., Photon-counting detector CT: system design and clinical applications of an emerging technology, Radiographics : a Review Publication of the Radiological Society of North America, Inc. 39 (3) (2019) 729–743, https://doi.org/10.1148/rg.2019180115.
[16] C. Hong, K.T. Bae, T.K. Pilgram, Coronary artery calcium: accuracy and reproducibility of measurements with multi-detector row CT–assessment of effects of different thresholds and quantification methods, Radiology 227 (3) (2003) 795–801.
[17] P.J. Pickhardt, L.J. Lee, del Rio A. Muñoz, et al., Simultaneous screening for osteoporosis at CT colonography: bone mineral density assessment using MDCT attenuation techniques compared with the DXA reference standard, J. Bone Miner. Res. 26 (9) (2011) 2194–2203, https://doi.org/10.1002/jbmr.428.

[18] S. Demehri, M.K. Kalra, F.J. Rybicki, et al., Quantification of urinary stone volume: attenuation threshold-based CT method–a technical note, Radiology 258 (3) (2011) 915–922, https://doi.org/10.1148/radiol.10100333.
[19] V. Koch, N.G. Hokamp, M.H. Albrecht, et al., Accuracy and precision of volumetric bone mineral density assessment using dual-source dual-energy versus quantitative CT: a phantom study, Eur Radiol Exp 5 (1) (2021) 43, https://doi.org/10.1186/s41747-021-00241-1.
[20] X. Li, X. Li, J. Li, et al., The accuracy of bone mineral density measurement using dual-energy spectral CT and quantitative CT: a comparative phantom study, Clin. Radiol. 75 (4) (2020), https://doi.org/10.1016/j.crad.2019.11.008.
[21] M. Wang, Y. Wu, Y. Zhou, J. Dong, P. Hou, J. Gao, The new fast kilovoltage-switching dual-energy computed tomography for measuring bone mineral density, Quant. Imag. Med. Surg. 13 (2) (2023) 801–811, https://doi.org/10.21037/qims-22-701.
[22] A. Euler, J. Solomon, A.E. Farjat, R.C. Nelson, E. Samei, D. Marin, High-pitch wide-coverage fast-kilovoltage-switching dual-energy CT: impact of pitch on noise, spatial resolution, and iodine quantification in a phantom study, AJR Am. J. Roentgenol. 212 (3) (2019) W64–W72, https://doi.org/10.2214/AJR.18.19851.
[23] R. Symons, T.E. Cork, P. Sahbaee, et al., Low-dose lung cancer screening with photon-counting CT: a feasibility study, Phys. Med. Biol. 62 (1) (2017) 202–213.
[24] B.W. Hoyt, A.E. Lundy, D.M. Clark, D. Colantonio, S.M. Tintle, B.K. Potter, Femoral neck Hounsfield units as an adjunct for bone mineral density after combat-related lower extremity amputation, J. Orthop. Trauma 35 (5) (2021).
[25] E.A.P.M. Romme, J.T. Murchison, K.F. Phang, et al., Bone attenuation on routine chest CT correlates with bone mineral density on DXA in patients with COPD, J. Bone Miner. Res. 27 (11) (2012) 2338–2343, https://doi.org/10.1002/jbmr.1678.
[26] Y.W. Kim, J.H. Kim, S.H. Yoon, et al., Vertebral bone attenuation on low-dose chest CT: quantitative volumetric analysis for bone fragility assessment, Osteoporos. Int. : a Journal Established as Result of Cooperation Between the European Foundation For Osteoporosis and the National Osteoporosis Foundation of the USA 28 (1) (2017) 329–338, https://doi.org/10.1007/s00198-016-3724-2.
[27] R.W. van Hamersvelt, A.M.R. Schilham, K. Engelke, et al., Accuracy of bone mineral density quantification using dual-layer spectral detector CT: a phantom study, Eur. Radiol. 27 (10) (2017) 4351–4359, https://doi.org/10.1007/s00330-017-4801-4.
[28] K. Mei, B.J. Schwaiger, F.K. Kopp, et al., Bone mineral density measurements in vertebral specimens and phantoms using dual-layer spectral computed tomography, Sci. Rep. 7 (1) (2017) 17519.
[29] W. Zhou, D.J. Bartlett, F.E. Diehn, et al., Reduction of metal artifacts and improvement in dose efficiency using photon-counting detector computed tomography and tin filtration, Invest. Radiol. 54 (4) (2019).
[30] T. Flohr, B. Schmidt, Technical basics and clinical benefits of photon-counting CT, Invest. Radiol. 58 (7) (2023).
[31] G.X. Ding, D.M. Duggan, C.W. Coffey, Accurate patient dosimetry of kilovoltage cone-beam CT in radiation therapy, Med. Phys. 35 (3) (2008) 1135–1144.
[32] J.-P. Grunz, J.F. Heidenreich, S. Lennartz, et al., Spectral shaping via tin prefiltration in ultra-high-resolution photon-counting and energy-integrating detector CT of the temporal bone, Invest. Radiol. 57 (12) (2022).
[33] S. Ohira, T. Karino, Y. Ueda, et al., How well does dual-energy CT with fast kilovoltage switching quantify CT number and iodine and calcium concentrations? Acad. Radiol. 25 (4) (2018) 519–528, https://doi.org/10.1016/j.acra.2017.11.002.
[34] L.N. Rothenberg, K.S. Pentlow, Radiation dose in CT, Radiographics : a Review Publication of the Radiological Society of North America, Inc. 12 (6) (1992) 1225–1243.
[35] M.M. Lell, M. May, P. Deak, et al., High-pitch spiral computed tomography: effect on image quality and radiation dose in pediatric chest computed tomography, Invest. Radiol. 46 (2) (2011) 116–123, https://doi.org/10.1097/RLI.0b013e3181f33b1d.
[36] F. Bamberg, R. Marcus, W. Sommer, et al., Diagnostic image quality of a comprehensive high-pitch dual-spiral cardiothoracic CT protocol in patients with undifferentiated acute chest pain, Eur. J. Radiol. 81 (12) (2012) 3697–3702, https://doi.org/10.1016/j.ejrad.2010.11.032.
[37] K. Martini, A. Meier, K. Higashigaito, N. Saltybaeva, H. Alkadhi, T. Frauenfelder, Prospective randomized comparison of high-pitch CT at 80 kVp under free breathing with standard-pitch CT at 100 kVp under breath-hold for detection of pulmonary embolism, Acad. Radiol. 23 (11) (2016) 1335–1341, https://doi.org/10.1016/j.acra.2016.07.010.
[38] T. Emrich, G. Aquino, U.J. Schoepf, et al., Coronary computed tomography angiography-based calcium scoring: in vitro and in vivo validation of a novel virtual noniodine reconstruction algorithm on a clinical, first-generation dual-source photon counting-detector system, Invest. Radiol. 57 (8) (2022) 536–543, https://doi.org/10.1097/RLI.0000000000000868.
[39] G. Apfaltrer, M.H. Albrecht, U.J. Schoepf, et al., High-pitch low-voltage CT coronary artery calcium scoring with tin filtration: accuracy and radiation dose reduction, Eur. Radiol. 28 (7) (2018) 3097–3104, https://doi.org/10.1007/s00330-017-5249-2.
[40] A. Hutt, A. Duhamel, V. Deken, et al., Coronary calcium screening with dual-source CT: reliability of ungated, high-pitch chest CT in comparison with dedicated calcium-scoring CT, Eur. Radiol. 26 (6) (2016) 1521–1528, https://doi.org/10.1007/s00330-015-3978-7.
[41] V. Zaichick, M. Tzaphlidou, Determination of calcium, phosphorus, and the calcium/phosphorus ratio in cortical bone from the human femoral neck by neutron activation analysis, Appl. Radiat. Isot. 56 (6) (2002) 781–786.
[42] S. Jang, P.M. Graffy, T.J. Ziemlewicz, S.J. Lee, R.M. Summers, P.J. Pickhardt, Opportunistic osteoporosis screening at routine abdominal and thoracic CT: normative L1 trabecular attenuation values in more than 20 000 adults, Radiology 291 (2) (2019) 360–367, https://doi.org/10.1148/radiol.2019181648.
[43] P.J. Pickhardt, B.D. Pooler, T. Lauder, A.M. del Rio, R.J. Bruce, N. Binkley, Opportunistic screening for osteoporosis using abdominal computed tomography scans obtained for other indications, Ann. Intern. Med. 158 (8) (2013) 588–595, https://doi.org/10.7326/0003-4819-158-8-201304160-00003.
[44] A.E. Papadakis, A.H. Karantanas, G. Papadokostakis, E. Petinellis, J. Damilakis, Can abdominal multi-detector CT diagnose spinal osteoporosis? Eur. Radiol. 19 (1) (2009) 172–176, https://doi.org/10.1007/s00330-008-1099-2.
[45] Q. Ma, Z. Yang, X. Han, F. Liu, D. Su, H. Xing, Influence of parathyroidectomy on bone calcium concentration: evaluation with spectral CT in patients with secondary hyperparathyroidism undergoing hemodialysis-A prospective feasibility study, Radiology 284 (1) (2017) 143–152, https://doi.org/10.1148/radiol.2016161797.
[46] A. Ferrero, R. Gutjahr, A.F. Halaweish, S. Leng, C.H. McCollough, Characterization of urinary stone composition by use of whole-body, photon-counting detector CT, Acad. Radiol. 25 (10) (2018) 1270–1276, https://doi.org/10.1016/j.acra.2018.01.007.